

Microstructural and Mechanical Evaluation of Laser-Assisted Cold Sprayed Bio-ceramic Coatings: Potential Use for Biomedical Applications

Monnamme Tlotleng, Esther Akinlabi, Mukul Shukla, and Sisa Pityana

(Submitted July 16, 2014; in revised form October 1, 2014)

Bio-composite coatings of 20 wt.%, HAP and 80 wt.%, HAP were synthesized on Ti-6Al-4V substrates using LACS technique. The coatings were produced with a laser power of 2.5 kW, powder-laser spot trailing by 5 s. The coatings were analyzed for the microstructures, microhardness, composition, and bio-corrosion using SEM-EDS, XRD, hardness tester, and Metrohm PGSTAT101 machine. SEM images indicated least pores and crack-free coating with dark-spots of Ti-HAP for the 20 wt.%, HAP as opposed to the 80 wt.%, HAP coating which was solid, porous and finely cracked and had semi-melted Ti-HAP particles. The EDS mappings showed high content of HAP for the 80 wt.%, HAP coating. The diffraction patterns were similar, even though the Ti-HAP peak was broader in the 80 wt.%, HAP coating and the HAP intensities were lower for this coating except for the (004) peak. The hardness values taken at the interface inferred that the 80 wt.%, HAP coating was least bonded. It was possible to conclude that when this phase material increased the hardness dropped considerably. The bio-corrosion tests indicated that the presence of HAP in coating leads to a kinetically active coating as opposed to pure titanium coating.

Keywords composite, hydroxyapatite, laser-assisted cold spray, laser power, titanium

1. Introduction

Metals and their alloys can be used in tissue engineering as permanent or temporary scaffolds. Metals such as stainless steel (SS) have good mechanical properties (stiffness, elasticity and ductility) that are necessary for the fabrication of long bone and screws, but they are prone to corrosion while they are non-biocompatible. For

this understanding, SS scaffolds are preferred only as temporary implants while cobalt alloys (CoCrMo) are favorable for orthopedics given that they are good electrical conducting materials and have better corrosion and fatigue-resistant properties. Unfortunately, CoCrMo have stiffness greater than that of SS and titanium alloy (Ti-6Al-4V), hence they have not been used successfully for the long bone replacement applications (Ref 1-3). Ti-6Al-4V is bioinert in that it does not form an immediate chemical bond with the natural bone upon implantation (Ref 4, 5). To date, Ti-6Al-4V is the most preferred material over all material-metal alloys used for the orthopedic applications (Ref 3-5) given its attractive features. The low cytotoxicity reported with Ti-6Al-4V is triggered by V ions which leach into the human blood system when the implant was left in service for long (Ref 6). V ions can cause long-term diseases such as Alzheimer's, neuropathy, and Osteomalacia (Ref 3). It is proposed that to prevent these post implantation diseases from occurring while inducing the Osseo-integration of Ti-6Al-4V implants, their surface properties must be altered by coating with hydroxyapatite (HAP) (Ref 7).

Hydroxyapatite is the most researched bio-ceramic material, in the field of biomedical engineering for scaffolds manufacturing, of all the calcium phosphate family (CaP); not because of its crystallographic similarities likened to the natural bone; but this is since HAP can induce osteo-conductivity and integrate the coated-metal implant with the natural human tissues in vivo (Ref 8-10, 11, 12). The attachment of implants with natural bones is possible since HAP is characterized by natural porosity in which the tissue

Monnamme Tlotleng, Laser Material Processing, National Laser Center CSIR, Pretoria 0001, South Africa and Department of Mechanical Engineering Science, University of Johannesburg, Auckland Park, Kingsway Campus, Johannesburg 2006, South Africa; **Esther Akinlabi**, Department of Mechanical Engineering Science, University of Johannesburg, Auckland Park, Kingsway Campus, Johannesburg 2006, South Africa; **Mukul Shukla**, Department of Mechanical Engineering, MNNIT, Allahabad 211004, UP, India and Department of Mechanical Engineering Technology, University of Johannesburg, Doornfontein Campus, Johannesburg 2006, South Africa; and **Sisa Pityana**, Laser Material Processing, National Laser Center CSIR, Pretoria 0001, South Africa and Department of Chemical and Metallurgical Engineering, Tshwane University of Technology, Pretoria 0001, South Africa. Contact e-mails: MTlotleng@csir.co.za and daopase@gmail.com.

can grow around and into the scaffolds. In addition to it being porous, HAP is also brittle, heat sensitive, and non-ductile. HAP possesses poor mechanical properties such as low plasticity, fatigue, and creep resistance (Ref 13). Due to the observed poor mechanical properties; brittleness and porousness, HAP may not be used as a bulk material for structural support, (Ref 14, 15, 16), except as a compressive material. As a compressive material, HAP coating can potentially suppress V ions, be flexible at the contact point with the implant, more so it will accelerate the attachment and growth of the human natural tissue around and into the metal scaffolds. The porous nature of HAP makes it possible that after Osseo-integration nutrition can flow within the scaffolds (Ref 7, 8, 17).

The heat sensitivity and lack of plastic deformation of HAP are of greater concern where this material limits the choice of surface coating techniques from which it can be deposited onto Ti-6Al-4V for biomedical applications. Even so, research continues to develop and establish other industrial acceptable methods from which HAP coatings can be fabricated on Ti-6Al-4V. Several techniques have been used successfully to modify the metallic surface of Ti-6Al-4V alloy by coating it with a thin, continuous layer of HAP (Ref 7, 10, 18, 19). Traditionally, HAP has been successfully deposited on Ti-6Al-4V using electrochemical (cathodic) deposition (Ref 20), Sol-gel (Ref 21), magnetron sputtering (9), pulse laser deposition (Ref 22, 23), laser cladding (Ref 24, 25), thermal spraying techniques (Ref 26), seeded hydrothermal deposition (Ref 14), cold spraying techniques (Ref 27, 28), Laser-engineered net shaping technique (Ref 8), and laser-assisted deposition methods (Ref 29). The most preferred method of producing thin, continuous films of HAP on base metals is plasma spraying. Plasma spraying is desirable for its high deposition rates efficiencies, making it an acceptable industrial technique to be used in depositing HAP coatings. Nonetheless, there is an evidence that proves definitively that the HAP coatings deposited with plasma and flame-based spray techniques contain decomposed phases of HAP. These decomposed phases [calcium oxide (CaO); α - and β -tricalcium phosphate (TCP) and tetra calcium phosphate (TTCP)] which are due to the high process temperatures involved during depositions affect the performance and life-span of the coating during service. The disadvantages and advantages of HAP coatings deposited with various techniques are presented and discussed in details by Doronzhkin (Ref 7).

Meanwhile, it is explained that wet deposition techniques cannot achieve thick, continuous HAP coatings making them expensive to operate and undesirable. Plasma spraying technique produces HAP coatings that are weakly bonding to the substrate at the interface, accelerated resorption during service and dilution. The delamination and rapid resorption of the coating during service are ascribed to the presence of the decomposed phases of HAP in the coating while the weakened bonding between the coating and the substrate is attributed to the vast thermal mismatches that exist between HAP ($13.3 \times 10^{-6} \text{ K}^{-1}$) and Ti-6Al-4V ($8.4\text{-}8.8 \times 10^{-6} \text{ K}^{-1}$) (Ref 30). To address the issues around the characteristics of

HAP coating produced with plasma spraying while reducing the process temperatures, cold spray (CS) technique was developed. CS is an industrial technique that retains all the advantages of plasma spraying. Consequently, CS cannot deposit pure HAP powder since it lacks the plastic deformation, a required characteristic for any material being cold sprayed. Meanwhile, CS techniques are cost ineffective since they require expensive process gas (Helium) and heating sources (Ref 31, 32). To overcome the shortcomings presented for both plasma and cold spraying techniques, during HAP deposition, many studies use bio-composite powders comprising a metal (typically Ti) and HAP. The metal in the composite is able to give strength to the HAP, and induce plastic deformation to HAP while reducing the thermal mismatching that exists between the Ti-6Al-4V substrate and HAP powder during deposition.

Both plasma and CS techniques have been used, by independent researchers, to deposit a bio-composite coating (Ref 4, 5, 9, 27-29). Plasma-sprayed bio-composite coatings yield with similar problems as presented before. CS is an alternative industrial technique to plasma spraying, even though it limits the number of powders which can be deposited and requires expensive processing gas like Helium (He) and heating source for the process to yield high deposition rates and be efficient. To circumvent the technical shortcomings present against CS techniques, laser enabling techniques are investigated. It is presented in (Ref 27) that CS can deposit bio-composite coating, but with reduced HAP content. The authors believe that laser-enabled CS techniques can improve on the quantity of HAP in the coating. This study therefore presents bio-composite coatings deposited with laser-assisted cold spray (LACS). LACS is an extension of CS and in no way do we believe it replaces CS at the industrial scale.

LACS is a new concept of CS techniques. LACS set-up comprises mainly a De Laval supersonic diverging-converging nozzle, a process gas and the powder particle entraining gas, and high power laser which serve as a heating source. The technical basics and the advantages of this technique over CS are discussed elsewhere by the corresponding author (Ref 32). LACS was first demonstrated by Bray et al. (Ref 31), in 2006, at the International Congress of Applications of Laser and Electro-Optics held in the United State of America. According to Lupoi et al. (Ref 33), during LACS deposition, a laser source preheat the substrate; hence therefore removing the oxide layer while being able to simultaneously preheat the powder-particles below melting point to temperatures that range between 30% and 70% of the particle melting point. This heat provides for the softening of the particles strength while allowing the particles to deform and build up the coating upon hitting the surface.

The effect of laser power during LACS deposition is the most studied phenomena. For example, Lupoi et al. (Ref 34) illustrated by means of micrographs how titanium powder can bond to the metallic substrate with an increase in substrate-powder temperature. Olakanmi et al. (Ref 32) studied the effect of laser on the deposition mechanism of aluminum powder. All reviewed studies support the initial analogy by Brodmann (Ref 35), and agree that the suffi-

cient energy provided by laser source during laser deposition can cause the oxide film surrounding the particles to be brittle and crack open during impact thereby leading to the formation of a surface coating (Ref 32, 35). To date, only Olakanmi et al. (Ref 32) and Bray et al. (Ref 31) have successfully produced metal coatings using high-pressure LACS systems, but nothing yet on bio-composites of Ti and HAP. In this study, a LACS technique was used to deposit bio-composite powders consisting of Ti and HAP. LACS bio-composite coatings presented in this study were named 20 wt.%, HAP and 80 wt.%, HAP. The microstructures of these coatings were studied using optical microscope and focal ion beam, scanning electron microscope capable of reporting on elemental analysis using electron dispersive spectroscopy (FIB, SEM-EDS). X-ray diffraction was used to match the phase identity of the feedstock powder to the coatings while Vickers' hardness machine and Metrohm PGSTAT101 were used to study the micro-hardness and bio-corrosion of the coatings, respectively.

2. Materials and Methods

A powder displayed by Fig. 1 was achieved by mechanically milling together a commercially pure (CP), spherical titanium (Ti) powder of particle size distribution 45-90 μm supplied by TLS Technik GmbH and HAP (90) of particles size 62.1 μm supplied by Plasma Biotol, United Kingdom. Steel balls were used to mechanically grinding (CP)-Ti and HAP (90) into a bio-composite powder. Two sets of powders, viz., 20 wt.%, HAP and 80 wt.%, HAP were produced. The powders were tested for flowability using FT4 Powder Rheometer which had a hardened stainless steel blade diameter of 24.5 mm and a borosilicate testing vessels having a diameter of 25 mm. The powder composition analyzed with FIB, SEM-EDS is shown in Fig. 1. Titanium alloy (Ti-6Al-4V) substrates of dimensions 70 \times 70 \times 5 mm³ were available for use as deposition surfaces. The substrates were initially sand-blasted to improve their adhesion properties.

2.1 LACS Set-Up

LACS equipment used in this study was located at the CSIR National Laser (NLC/CSIR), Pretoria, South Africa. The set-up included a 4.4 kW, 044 Rofin Nd:YAG (Rofin DY 044) laser system of 1.06 μm wavelength, a AT-12000HPHV 5000PSI (35 bar) powder feeder (Thermach Inc., Appleton), compressed Nitrogen bulk gas tank with controlled regulation and a de Laval supersonic nozzle. The converging-diverging (de Laval) DLV-180 nozzle used in this study was manufactured and supplied from the Centre for Industrial Photonics, Institute for Manufacturing, University of Cambridge, UK. Figure 2 shows this equipment.

Figure 2 shows the equipment used to set-up the LACS used in this study to deposit the bio-composite powders.

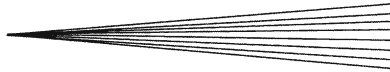


Figure 2(a) shows the in-let and out-let of the high-pressure Nitrogen (N₂) gas that was used as both the entraining and processing gas. Regulators, pressure gages and the taps were attached to both ends of the gas lines. The gas on the left side was the entraining gas and connected to the Thermal high pressure, regulated powder feeder that had a releasing, venting valve (Fig. 2b). The gas on the right-hand side connected to the De Laval, supersonic diverging-converging nozzle shown in Fig. 2(c). The powder stream and the N₂ gas recombined inside the nozzle were accelerated through the nozzle at high supersonic speeds. The nozzle was mounted on the Kuka robot arm which allowed for the simultaneous scanning of the laser source spot and the powder spot across the depositing surface. A well optimized laser-powder spot is characterized by the spot that has the laser spot locking within it the powder spot (See Fig. 2). This step allows for the powder to be fully preheated and deposit efficiently. The bio-composites coatings presented in this study were achieved by allowing the powder-jet stream to trail behind the laser spot by 15 mm with a delayed time of 1.5 s. Such a spot is shown in Fig. 3.

Figure 4 and 5 illustrate the phenomena of LACS coating and the actual process set-up that was used in this study. Figure 4 shows powder-laser interaction, melted and unmelted powder particle, and the base metal without dilution. Figure 5(c) shows the nozzle mounted on the Kuka robot arm, the process chamber and the bracket that held the nozzle on the set angle. In this study, the nozzle was held perpendicular to the substrate at the stand-off distance of 50 mm while the laser beam was inclined at 15° and the laser-powder spot traverse speed, laser power, and the deposition pressure were kept constant at 30 mm/s, 2.5 kW, and 16.5 bars, respectively. The choice of the laser power was based on the deposition characteristics of (CP)-Ti coatings.

2.2 Sample Analysis

The produced coatings were sectioned then ground and polished to a 0.04 micron (OP-S suspension) surface finish with a Struers TegraForce-5 auto/manual polisher. Post polishing, the selected coatings were etched with Kellers' reagent for 3 min and then analyses for microstructures using light optical microscope connected to the Analysis® software. The best samples were analyzed with Auriga, CrossBeam FIB Workstation with GEMINI FESEM column equipped with The Oxford X-Max instrument with 20-mm square window, Aztec Software. Imaging by SEM allowed for in-depth microstructural analyses. Also, SEM-EDS component was used to characterize samples for their composition. The phase present in the coatings was analyzed with Panalytical XPert PRO PW 3040/60 x-ray diffraction (XRD) with Cu K α monochromator radiation source. The mechanical micro-hardness values of the coatings were conducted using Matsuzawa Seiko Vickers micro-hardness tester model MHT-1. An indenting load of 300 g and a 10 s dwell time were used for each hardness indent action. The selected bio-ceramic coatings were sent for bio-corrosion analysis using Metrohm PGSTAT101.

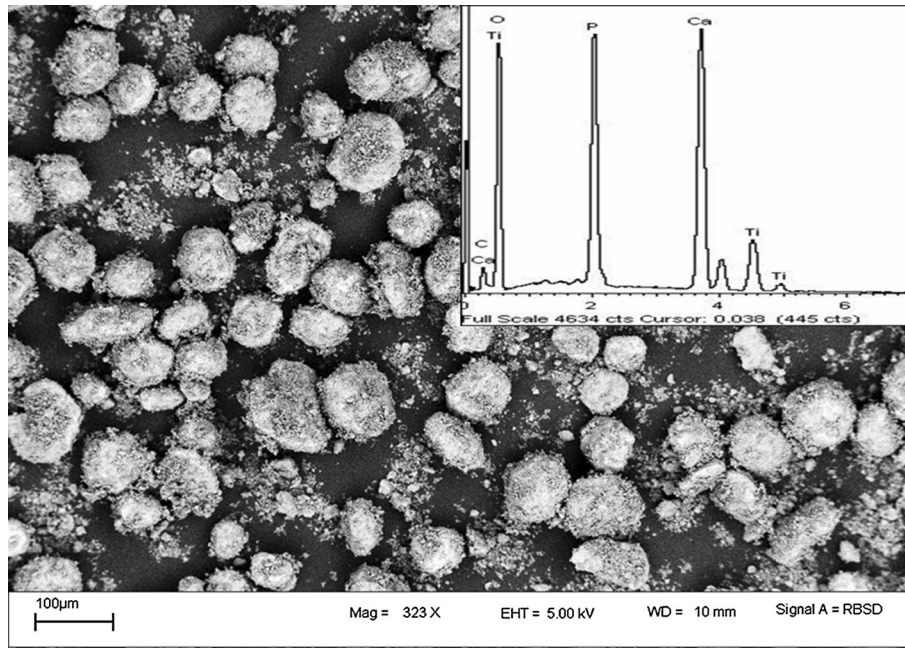


Fig. 1 Morphology and composition of the Ti-HAP powders used in this study

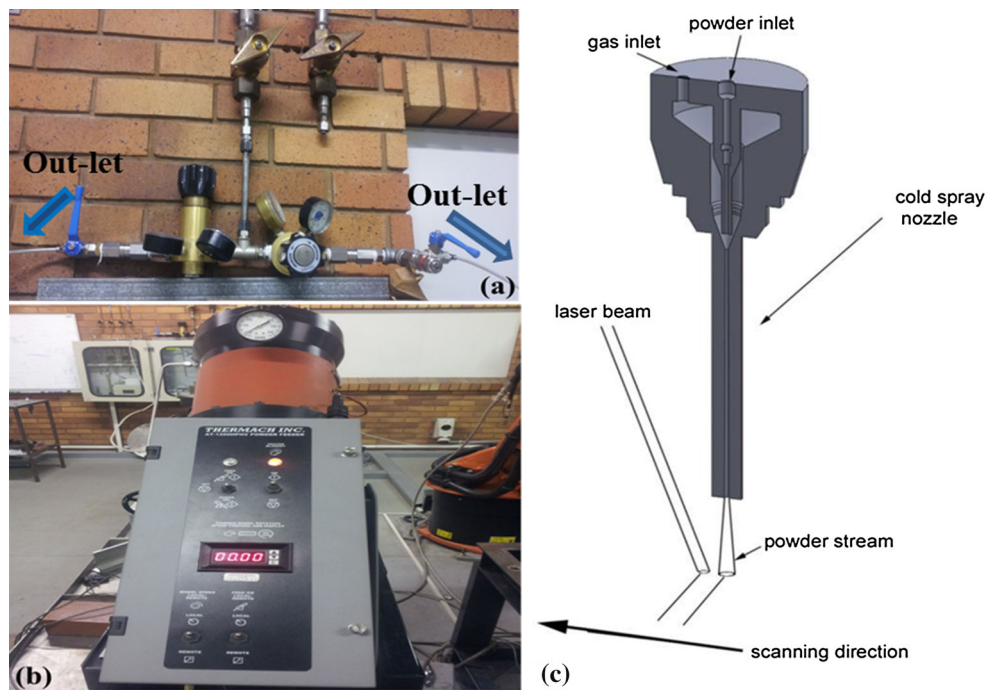


Fig. 2 Equipment used to set-up LACS system

3. Results and Discussion

3.1 LACS Coatings Microstructures

LACS technology has recently surfaced as a metal depositing technique for surface coat making. In this regard, it is now evident that the open literature is scant of microstructures or nay scientific results relating to HAP or

bio-composite coatings that were fabricated using LACS. However, there are results from the literature presented on these types of coating, but from traditional cold spray and plasma spraying techniques. Given this understanding, the results reported in this study were compared or contrasted to the results that were presented on both plasma and cold spray techniques. The results reported

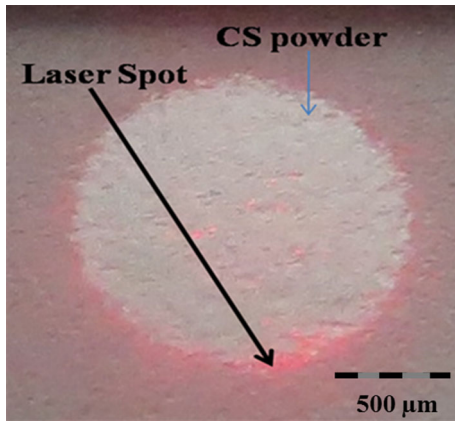
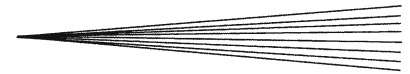


Fig. 3 Optimized powder-laser spot interaction

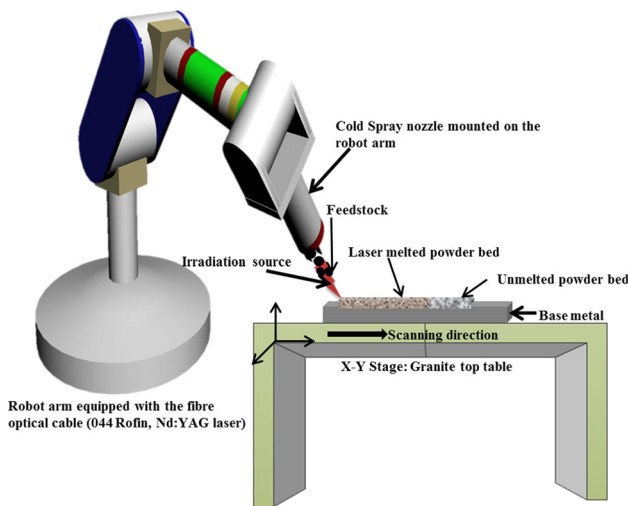


Fig. 4 The LACS process illustration

here are on the coatings of 20 wt.%, HAP and 80 wt.%, HAP deposited with the LACS technique.

3.1.1 20 wt.%, HAP LACS Coating. The LACS deposited coating that contained 20 wt.%, HAP is presented in Fig. 6.

Figure 6(a) reports the as-deposited 20 wt.%, HAP coating. Distinctively, it is possible to identify the Ti-6Al-4V substrate, the coating, and the dark spots which are formed by the partially melted particles which appear as a filling. To reveal the microstructures of the coating, the as-received coating was etched with Kellers' reagent for 3 min (Fig. 6(b)). It is possible to see from Fig. 6(b) the dark spots, sought of filled holes, both inside the coating and at the interface between the coating and the substrate. The fine white bands (splats) present could only be from the HAP material in the composite powder. These splats are highly concentrated at the top most half of the coating and appears as channel filets at the bottom half of the coating. Also, the observed HAP bands are present around the observed dark-spot on the coating. Scanning electron microscope image of the dark spot is shown by Fig. 6(c). From this figure it is possible to conclude that

these particles are a mixture and are almost loose or semi-melted. The white particles are normally referred to as Ti while the dark phases are HAP. Accepting this analogy, it was possible to assume that Ti was the most unmelted material (loose) while HAP was the semi-melted material present in the "hole." The EDS taken on this filet indicated the presence of both Ti and HAP and concluded a high content of Ti as opposed to HAP.

3.1.2 80 wt.%, HAP LACS Coating. The LACS deposited coating that contained 20 wt.%, HAP is presented in Fig. 7.

Figure 7(a) is the as-produced 80 wt.%, HAP coating. Likewise the 20 wt.%, HAP coating, it is possible to distinguish between the substrate and the coating. The coating had dark-spot inside the coating. Unlike in the case of the 20 wt.%, HAP coating, this coating has solid bonding which is not hindered by the broken particles. That is, the dark-spot is close to the bonding but is not forming an interface between the coating and the substrate as seen with the 20 wt.%, HAP coating. Figure 7(b) shows the microstructure of the deposited coating after etching for 3 min in Kellers' reagent. Three distinct features can be deduced from Fig. 7(b). These features include the brownish material which is etched Ti, the splats which is HAP, and the dark-spot filled with some particles. The observed splats are different from those reported by Khor et al. (Ref 36). The SEM images on the dark-spot concluded a bright, light phase material and melted dark-particles. The EDS mapping concludes that the presence of both Ti (bright phase) and HAP (dark-black phase) phases made the spot. The high magnification image of the white splats is shown by Fig. 7(d). The splats show fine cracks on the surface which can be attributed to the natural brittleness of HAP particles. Synonymously, the coating is highly porous. Contrary to the 20 wt.%, HAP coating, EDS results concluded high content of HAP for this coating.

3.2 Phase Analysis with X-ray Diffraction

Figure 8 compares 20 wt.%, HAP powder to its LACS coating. A similar representation of the phase composition in the two materials is observed. The only difference is the new peak observed at about 43° (TiO) and a shift of the TiO₂ peak from 36° in the powder to 38° in the coating. The peak identification shows that the diffraction peak of both Ti and HAP were preserved at exactly 31.77° and 40.170° peak positions, respectively. This observation relates to the processing temperatures. Typically, high processing temperatures lead to the decomposition of HAP in the coating. In this study, it becomes obvious that the chosen laser power, the parameters setting and the option to allow the powder and the laser source beam to trailing led to processing temperatures below melting point of the powder that led to the preservation of the initial properties of the powder.

In plasma spraying, HAP decomposition is associated with high processing temperatures and highly reactive atmospheres. To avoid the occurrence of HAP decom-



Fig. 5 The LACS process set-up used in this study

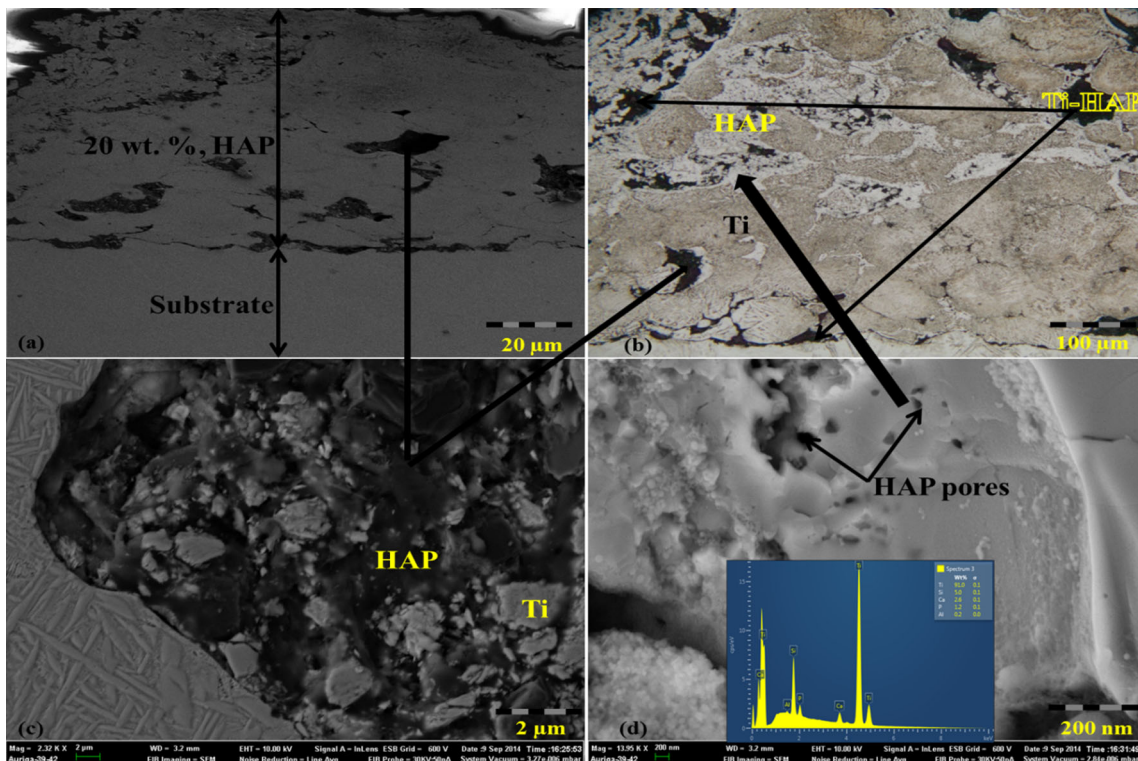


Fig. 6 20 wt.%, HAP LACS coating

position in plasma, deposited HAP particles should be deposited with little time interaction between the powder plume and the laser heat. LACS deposition achieves non-

decomposed phase of HAP in this study since during deposition the interaction time between material, substrate and laser heat were short-lived.

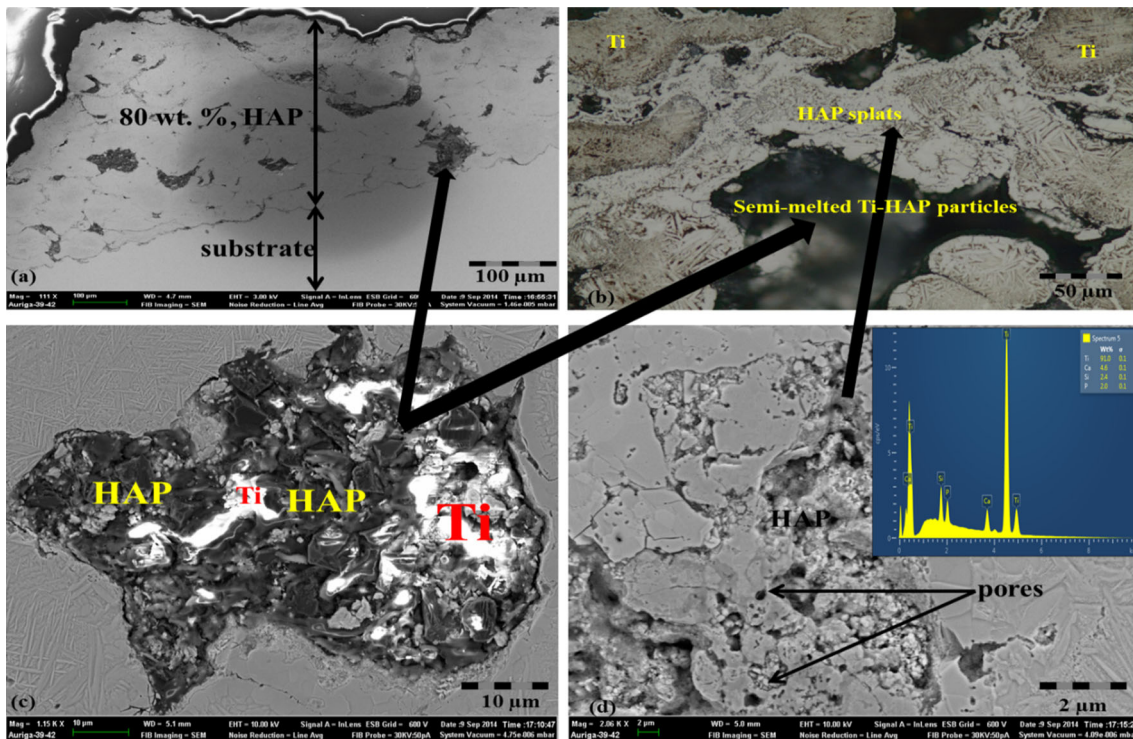


Fig. 7 80 wt.%, HAP LACS coatings

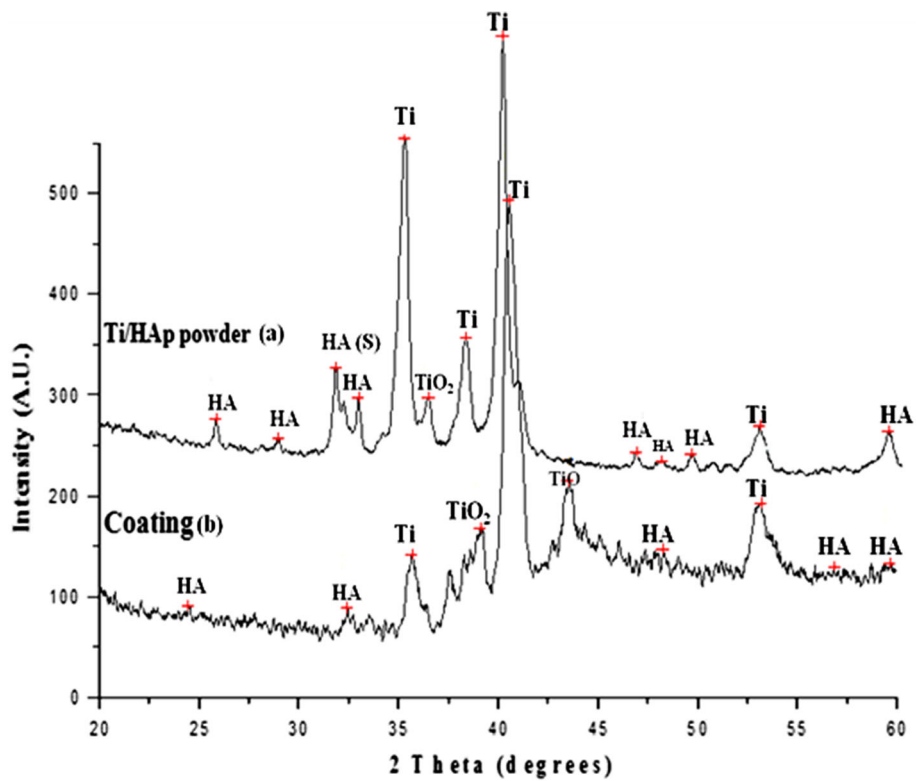


Fig. 8 Diffraction pattern comparing the 20 wt.%, HAP powder to its LACS coating

In addition to the preserved HAP and Ti diffraction peak, TiO and TiO₂ peaks are observed. TiO₂ peak is present in both the powder and the coating. This peak generally indicates an excess oxygen environment, but for this study the powder was milled under a high argon-controlled environment which depleted the oxygen while during deposition the process took place in a close chamber. The presence of the TiO₂ peak in both the powder and the coating cements the proneness of Ti to the oxygen which is typically accelerated by increasing the deposition environment temperatures above room temperature. TiO is an indication of low processing temperature and the reduction of TiO₂ by Ti in the oxygen depleted environments. Also to note is the broadening and the dropping in the peak intensity of Ti, TiO₂ and HAP in the coating. These effects are generally associated with the decomposition of HAP in the precursor powder. But, since it is already inferred and deduced from Fig. 4(a) that low processing temperatures were achieved during deposition, and that no obvious decomposition phases of HAP are observed, it becomes plausible that in the coating there maybe such phases of HAP which are limited and of low diffraction intensity which makes it difficult to be picked during analysis. This observation is already reported by Zhou et al. (Ref 5).

Figure 9 compares the LACS coating of 80 wt.%, HAP to the deposited powder.

Obviously, it is difficult to identify the peaks of the coating in this comparison since the intensity of the coating dropped considerably. However, it is possible to note that the two compared graphs follow similar trends. For example, the α -Ti/HAP peak positioned at 40.1 (100) is present in both peaks. However, this peak is broad in the coating, likewise the peak at position 42° which corresponds to HAP (302). To better understand the information presented in Fig. 9, it became necessary to compare the XRD data for both coatings. This comparison is presented in Fig. 10. Figure 10 reveals that the peak intensities of the HAP in the 80 wt.%, HAP are low, but all the anticipated peaks are present. These peaks are those with miller indexes (211) (300) (420) for HAP and α -Ti (101) at 40.1. The peaks (310) and (004) are more intense. The observation where the normal weak intensity peaks become more intense than the usual strong peaks for HAP material has been reported before (Ref 37). This occurrence is normal for HAP coatings produced with lasers and is attributed to the existence of TTCP in the coating, which has a crystallographic structural epitaxy similar to that of the HAP. To further establish the similarities and differences in the produced coatings, their XRD phase matches were compared. The comparison of the coatings is presented in Fig. 10.

Figure 10 identifies the presence of both HAP and Ti in the coating. The (211) peak which corresponds to HAP is well defined in 20 wt.%, HAP as opposed to the 80 wt.%, HAP coating. The α -Ti (100) peak is well defined for both coatings, but lower in intensity for the 80 wt.%, HAP coating. The α -Ti/HAP peak in position 42° is broad in the 80 wt.%, HAP coating. Generally, the two XRD patterns

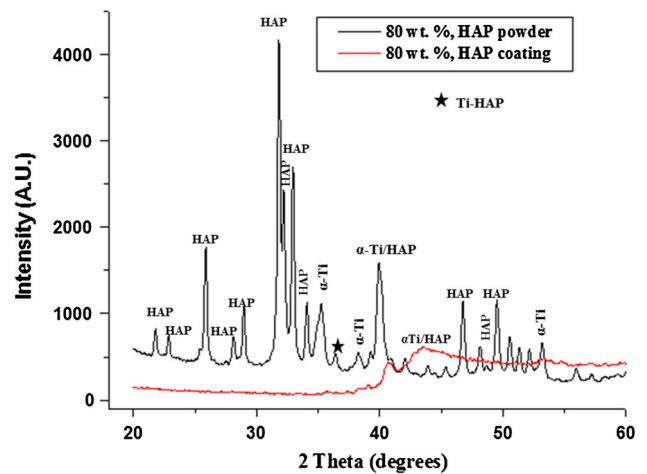


Fig. 9 Diffraction pattern comparing the 80 wt.%, HAP powder to its LACS coating

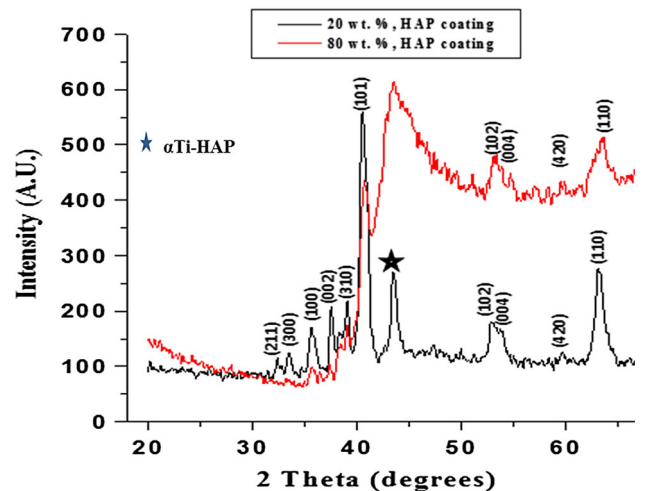


Fig. 10 XRD patterns of the 20 wt.%, HAP and 80 wt.%, HAP LACS coating

show similarities for both coatings even though the 80 wt.%, HAP coating has all the major HAP peaks at low intensities.

3.3 Mechanical Micro-Hardness Profiles

Figure 11 shows the picture of the indents that were taken across the surface of the coatings. Typically, the hardness data seek to qualify the mechanical properties of the coatings (Ref 16). More importantly, hardness values taken at the interface between the coating and the substrate are necessary to infer the bonding ability of the coating to the substrate. The higher the hardness values at the interface, the most bonded is the coating to the substrate. We anticipate that the hardness values will be high at the top of the clad, most high in the heat-affected zone and low on the substrate. Also, hardness must be signifi-

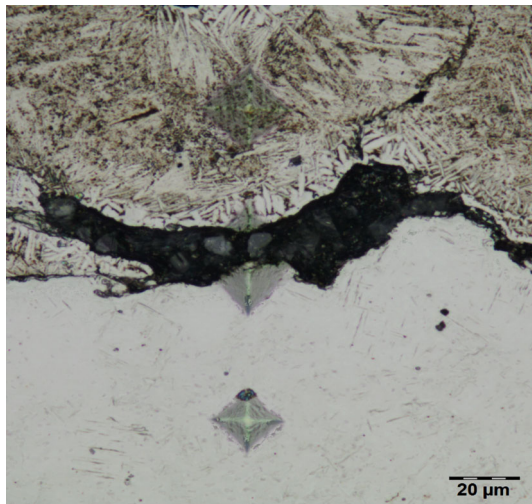


Fig. 11 Indentation profile taken across the surface of a LACS coating

cantly low around the cracks and pores. The hardness profiles of the investigated coatings are given in Fig. 12.

Figure 12 shows the Vickers hardness profiles of the LACS produced coatings. Both 20 wt.% HAP and 80 wt.% HAP coatings are shown. Four distinct areas of interest are highlighted on the figure. The top area relates to the surface and top most part of the coating. It can be deduced from the figure that the two coatings behaved similar at the top most half part. That is, the hardness profiling is of similar trend. The hardness was initially high and dropped linearly between 50 and 150 μm , more so with the 20 wt.% HAP coating. The hardness of the coating, at position 200 μm , is increased considerably (linearly). This area is known as the heat-affected zone. The similarities in the increase in the hardness values in the middle of the coating are understandably not misleading since both coatings were deposited using 2.5 kW laser power, similar scan speed, and a delay time of 15 s between powder and laser source heat. However, the HAZ hardness value for the 80 wt.% HAP is two times higher than that reported for the 20 wt.% HAP coating. This observation is in favor of the phenomena that support that Ti powder in composite leads to the reduction in the thermal expansion co-efficiency between HAP and Ti-6Al-4V during deposition. Similarly, the hardness values of both coatings, in the middle, decreased linearly. The hardness observation made this far deduce that these coatings were deposited under similar process conditions. Nonetheless, the hardness value at the interface indicated that the 20 wt.% HAP coating seems to be mostly well bonded to the substrate when compared to the 80 wt.% HAP coating. Similar observation has been reported by Mansur et al. (Ref 31). The observation made in this study that the hardness values, at the interface, increased from 20 wt.% HAP coating to 80 wt.% HAP coating could

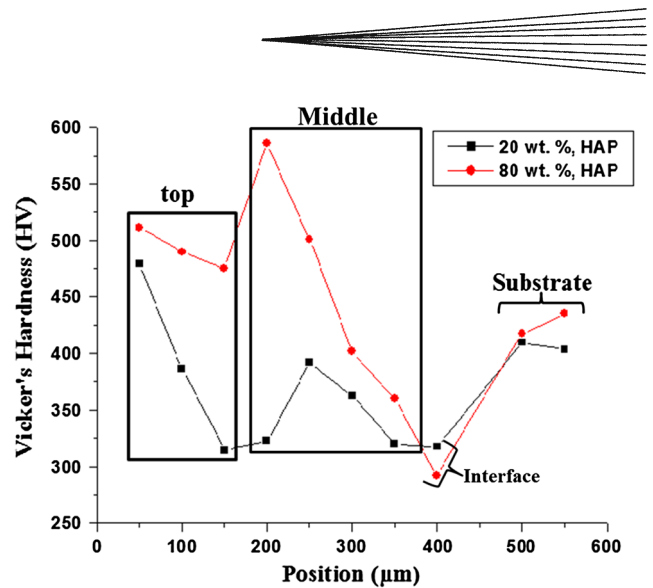


Fig. 12 Hardness profile of the LACS coatings

indicate that Ti-HAP powder matrix was such that HAP grew within Ti matrix in coatings. This observation is acceptable and can be supported by results presented in Fig. 6(b) and (c) and 7(b) and (c). In fact, the encapsulation of HAP by Ti matrix is best shown by Fig. 6(b). These results corroborate those reported by Choudhuri et al. (Ref 27). Since HAP is known to be easily affected by heat, the drop in the hardness values at the interface is ascribed to the rapid heating/cooling rates closer to the base metal where the molten Ti particles are able to entrap the HAP particles thereby being able to form the desired metallurgical bonding during cooling. Choudhuri et al. (Ref 29), during cold spraying, concluded that it is best to use small amount of HAP in composite (30% or less).

Figure 13 presents the indents taken at different phases of the coating.

Figure 13 explains in detail the results presented in Fig. 12. It became clear that hardness of the coatings presented is different in different phases of the coating. The indents presented by Fig. 13 show that the hardness of the coating was different for the substrate, the dark-spot, the brown phase, and the white “splats of HAP” phase. Figure 13(a) concludes that the dark-phase (HAP-Ti) material was softer than the substrate and the dark-brown material which were Ti-6Al-4V and titanium needles, respectively. Figure 13(b) definitely proves this observation. The indents were taken at the interface on the spot while observing the sizes of the pyramids with the increase of dark material (HAP) at the interface. What we observed is the decrease in hardness with an increase in the dark-phase material. Figure 13(c) shows the cracks on the indents taken on the white phase grown around the dark-phase material and the titanium dendrites. However, indents taken on the dense HAP “white splats” were very hard where it was not possible to even make the structure

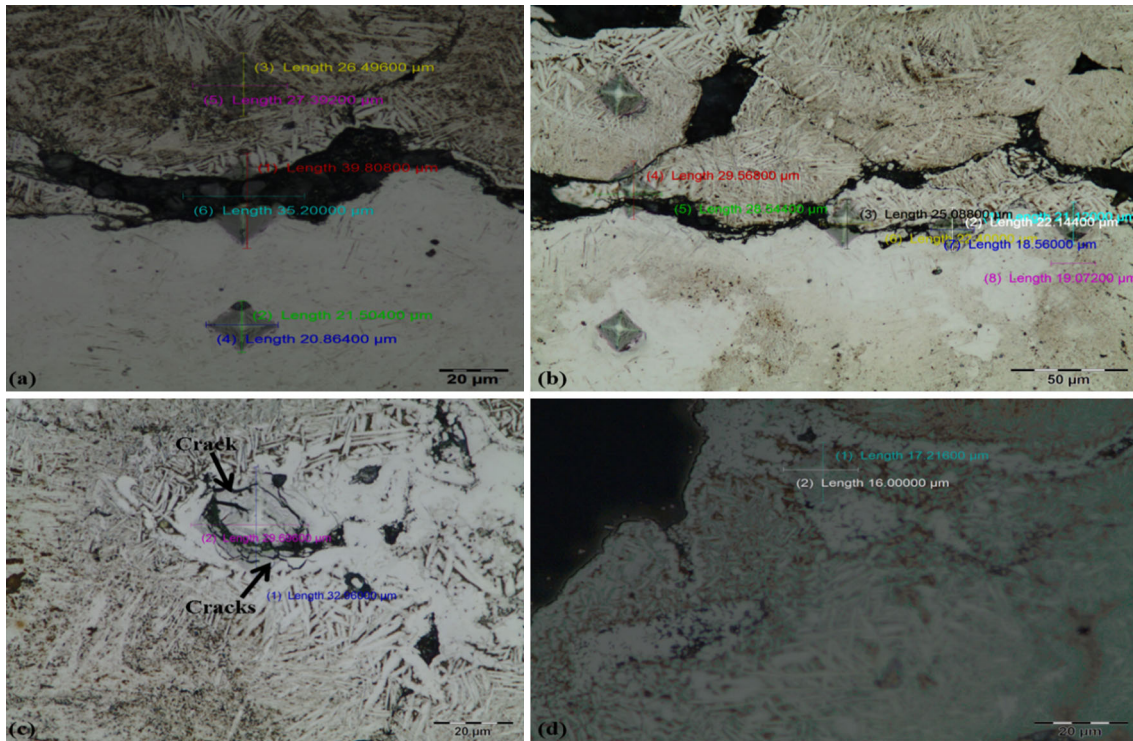


Fig. 13 Indents taken at different phases of the coating

of the indent (Fig. 13d). This observation is consistent since HAP is a ceramic and is most hard in which case it could not be penetrated by a pin loaded at 300 g. These results showed definitively that the dense white splats are most hard followed by the substrate while the HAP white bands that formed channels within the titanium dendrite matrix cracked during load with the dark-phase material (HAP filled) being the least hard.

4. Bio-corrosion

Figure 14 illustrates the thermodynamic and kinetic reactivity of the LACS Ti coating and the bio-composite coatings (20 wt.% HAP and 80 wt.% HAP) when they come into contact with Hank's solution.

From Fig. 14, it can be deduced that the 80 wt.% HAP coatings have the highest corrosion potential of -1.3 mV followed by pure titanium (pure Ti Reference) at -1.45 mV and then 20% wt.% HAP which has corrosion potential of about -1.75 mV. Similar results were reported by Zhou et al. (Ref 5) and Zhou et al. (Ref 28). Ti showed a huge oscillation in potential in the region ranging between -0.5 and -0.8 mV. The potentiodynamic results shown for Ti (Reference) are different from those reported in Ref 5. The behavior shown here by pure Ti coating corresponds to those reported for 20 wt.% HAP plasma-sprayed coating (Ref 5). Similarly, the 80 wt.% HAP coating showed the passivity behavior in the potential region ranging between -0.3 and -0.15 mV while

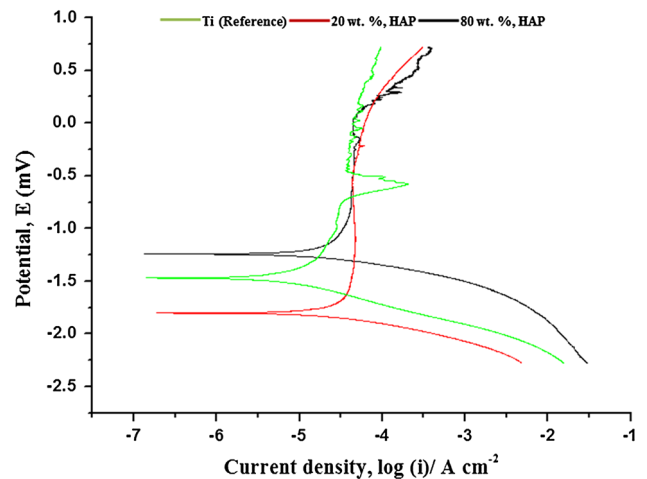
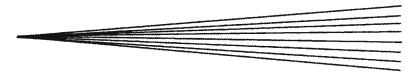


Fig. 14 Bio-corrosion of the LACS coatings

the 20 wt.% HAP remained thermodynamically more stable in the Hanks' solution. Both the bio-composite coatings show passivity in current in the range -4.5 to -3.5 cm^{-2} . Similar results are reported by Zhou et al. (Ref 28). Generally, these results show similar behavior for the bio-composite coatings which are most stable in the Hanks' solution as opposed to the LACS coating of the pure Ti (Reference). These observations proving definitively that HAP is able to improve the thermodynamic properties of the pure metal when they come in contact with the human blood.



5. Discussions

The 20 wt.%, HAP coating was characterized of fine bands of HAP splats that were like channels grown within the titanium matrix. In addition, this coating was observed to have splats that were concentrated at the top most part of the coating. Contrary to the fine bands of HAP that were observed for the 20 wt.%, HAP coating, the 80 wt.%, HAP coating had thin, porous continuous splats of HAP. Khor et al. (Ref 36) investigated the significance of melt-fraction of sprayed HAP using HVOF technique. There are similarities and differences between the splats observed here and those that were reported by Khor et al. The splats seen here are fully melted as opposed to being partially melted, indicating that the choice of the laser power was enough to generate heating necessary to transform the HAP particles from solid state to softened material before impact. The observed splats are both porous, which is typical for HAP. Porous splats of HAP are reported by Li et al. (Ref 38). Meantime, it was possible to identify the black-dark spots around which the melted HAP splats had grown (See Fig. 6 and 7). Khor et al. (Ref 36) illustrated the phenomena of melt fraction in particle. Obviously, from their results it was possible to conclude that which of the coatings (either 20 wt.%, HAP or 80 wt.%, HAP) had the particles in the observed dark spot having been almost completely melted. Evidently, the 80 wt.%, HAP coating seemed most melted according to observation that is deduced from Fig. 7(c).

The EDS results indicated that these particles were consisted of Ti and HAP. The HAP was the dark material in the spot while Ti was bright material under the objectives. Similar results have been reported by Li et al. when they investigated the formation and microstructure of thermally sprayed HAP/Titania bio-composite. TiO_2 was found to be unmelted and was the bright white round particle found within the coating. The coating which had TiO_2 was similar to that of the 20 wt.%, HAP coating. Nonetheless, the EDS results taken across the surface of both coatings indicate that HAP (CaP) content was high in the 80 wt.%, HAP as opposed to the 20 wt.%, HAP. Using the same highly resolved images, it was possible to see that the dark-spot material was highly concentrated at the interface between the coating and the substrate for the 80 wt.%, HAP coating. The 20 wt.%, HAP coating (Fig. 6(d)), on the surface, was flake-like, least porous, and crack free. These coatings are similar in appearance to the plasma-sprayed HAP coatings while the 80 wt.%, HAP coating was solid had fine cracks and most porous similar to the coatings reported by Li et al. using HVOF spraying technique.

The diffraction patterns of the coatings indicated that the HAP structure was intact in both coatings. TiO_2 was detected for the 20 wt.%, HAP coating, but no other decomposed phases were observed, particularly for the HAP. TiO_2 corresponds to the process temperature, however given that no decomposed phase of HAP was detected it is possible to infer that the temperatures were below the melting point of both the substrate and the

powder. Meanwhile, the diffraction patterns of both coatings were compared and showed similar trend, even though the Ti-HAP diffraction peak intensities for the 80 wt.%, HAP coating were broader and the HAP peaks located at the lower 2θ peaks were significantly lower in intensities, except for the HAP peak (004) at position 53° . This trend has been observed before and it is attributed to the presence of TTCP in the coating. TTCP has a similar diffraction patterns and atomic packing as pure HAP.

The hardness results were taken across the surface of the coating and at different phases present in both coatings. Initially, it was possible to see that the hardness was high at the top and dropped linearly inward the middle of the coating until at the substrate. Likewise, it was possible to conclude that different parts of the LACS coatings exhibited different hardnesses. The perplexing observation was one reported for the indents taken at the interface between the coating and the substrates. The hardness of the 80 wt.%, HAP on the surface (top part) was higher than the 20 wt.%, HAP coating. This is not surprising since a well-melted HAP particle will form a union with titanium during rapid cooling and solidification. Meanwhile, the observed white splats “HAP material” was not penetrable by the pin loaded at 100 g force, indicating that they were most hard, but the splats that occurred within the Ti matrix and around the dark-spot when indented cracked, showing weakness at this load. Khor et al. reported a hardness value of 532.3 HV for the unmelted splats while this study can reveal that the hardness values for the splats in the 80 wt.%, HAP and 20 wt.%, HAP coatings were 600 and 380 HV, respectively. The hardness values at the interface for the 80 wt.%, HAP were lower when compared to that of the 20 wt.%, HAP. This observation was ascertained by indenting the different phases present in the coating. The dark-phase spots that were initially observed were dominated at the interface of the 80 wt.%, HAP coating as opposed to the 20 wt.%, HAP coating. This phase was found to be least hard hence the hardness at the interface was decreased for the 80 wt.%, HAP coating (314.3 HV) when compared to the 20 wt.%, HAP coating (386.2 HV). The average hardness for the coating was 305.8 HV (top) and 414.1 (middle) for the 20 wt.%, HAP coating, and 391.5 HV (top) and 500.0 HV (middle) for the 80 wt.%, HAP coating. Khor et al. reported average hardness of 175.4 and 604.7 HV for their HVOF-sprayed HAP coatings.

The bio-corrosion tests showed that both coatings were thermodynamically more stable in the Hanks' solution as opposed to the pure titanium coating. Moreover, the presented bio-composite coatings showed similar current passivity which increased in the region -4.5 to -3.5 cm^{-2} while pure titanium coating showed a big oscillation in potential in the range -0.5 to -0.8 mV . Even though both coatings had similar corrosion current, indicating therefore that they both are kinetically active in Hanks' solution, 80 wt.%, HAP coating had corrosion potential twice high than that of the 20 wt.%, HAP coating. This observation indicating that the 80 wt.%, HAP is most favorable for biomedical applications. Corrosion current at the given

corrosion potential is an indication of the equilibrium state where mass transfer from the coating to solution is in equilibrium. For this study, we can consider that the Ca^{2+} and the phosphorus ions are migrating from the coating into the Hanks' solution until equilibrium is reached and there is no further exchange. The faster the rate of exchange, the faster and more quickly the coating is consumed and will lead to premature failure. This occurrence is mainly controlled by the pores. A porous coating will fail quicker, but since no pores were identified within both coatings, it was necessary to conclude that both coatings are necessary for the intended applications. In the meantime, the formation of the apatite layer is controlled by HAP hence the vast difference in the corrosion current that was observed between pure titanium coating and the 20 wt.%, HAP coating definitively proved that HAP is kinetically most active in Hanks' solution hence it had high corrosion current when compared to the pure titanium coating. Choudhuri et al. (Ref 27) made an observation that surfaces of a metallic implant need not to be entirely covered with HAP for it to be bio-integrable and be most favorable for the bio-medical applications. This observation is cemented here by the 20 wt.%, HAP.

6. Conclusion

This study demonstrated that bio-composite powders can be deposited with laser-assisted cold spraying technique. The 20 wt.%, HAP coating with fine bands of HAP grown within the Ti matrix was kinetically active likewise the 80 wt.%, HAP coating as opposed to the pure titanium coating. This observation concluded that HAP is kinetically active and fine bands of the HAP can induce Osseointegration during implantation. The HAP-Ti dark spot seeks to control the hardness of the coating at the interface hence the 80 wt.%, HAP was least bonded when compared to 20 wt.%, HAP coating which did not have this phase dominating at the interface between the coating and the substrate. It became clear that the more the content of the partially Ti-HAP at the interface, the hardness dropped considerably. Overall, it is the consideration of this study that both the LACS bio-coatings presented here will promote bio-integration as opposed to pure titanium coatings.

7. Future Work

In future, we wish to establish a fully functional processing window for the deposition of Ti-HAP powder at different levels of HAP in composite. A Taguchi approach will be undertaken. In addition, we seek to establish the behavior of coatings when they are soaked in SBF when the human body temperature will be mimicked. The work assumes that pre-heating of powder by lasers is necessary to lead to softening and actual deposition of a bio-composite powder. Already, the HAP crystals were observed at day 6 in which case it would be wise to use FIB-SEM to pick a lamella and characterize it with both TEM and XRD so that the material

characteristics before and after soaking can be ascertained. Fortunately, the effects of heat on HAP particles are known, but there is nothing on bio-composite powders made of Ti and HAP. This study will use DSC-TGA to study the evolution peaks of these composite. In part it will be able to account for the unmelted particles that are reported here while establishing heating profiles that are necessary for the development of procedures that will lead to a well consolidated HAP coating that has not decomposed.

Acknowledgments

The authors wish to give cognisance to the National Research Fund (NRF) and the Council for Scientific and Industrial Research (CSIR) of South Africa for their continued financial and resources support. Colleagues at the CSIR National Laser Centre, Laser Material Processing Group are thanked for their kindness and support, in particular Tebogo Mathebula and Khoro Malabi who helped with material preparation. Most importantly, the contribution and insightfulness of Dr. Eyitayo Olakanmi are mostly appreciated and recognized. Mr Lucas Mokwena helped with the experimental setup for that we acknowledged is generosity and willingness to assist.

References

1. R. Geetha, D. Durgalakshmi, and R. Asokamani, Biomedical Implants: Corrosion and its Prevention—A review, *Recent Pat. Corr. Sci.*, 2010, 2, p 40-54
2. M.B. Nasab and M.R. Hassan, Metallic Biomaterials of Knee and Hip: A Review, *Trends Biomater. Artif. Organs.*, 2010, 24(1), p 69-82
3. R. Geetha, A.K. Singh, R. Asokamani, and A.K. Gogia, Ti Based Biomaterials, the Ultimate Choice for Orthopaedic Implants-A Review, *Prog. Mater. Sci.*, 2009, 54, p 397-425
4. G. Zhao, L. Xia, G. Wen, L. Song, X. Wang, and K. Wu, Microstructure and Properties of Plasma-Sprayed Bio-coatings on a Low-Modulus Titanium Alloy From Milled HA/Ti Powders, *Surf. Coat. Technol.*, 2012, 206, p 4711-4719
5. X. Zhou, R. Siman, L. Lu, and P. Mohanty, Argon Atmospheric Plasma Sprayed Hydroxyapatite/Ti Composite Coating for Biomedical Applications, *Surf. Coat. Technol.*, 2012, 207, p 343-349
6. R. Banerjee, S. Nag, and H.L. Fraser, A Novel Combinatorial Approach to the Development of Beta Titanium Alloys for Orthopaedic Implants, *Mater. Sci. Eng. C.*, 2005, 25, p 282-289
7. S.V. Dorozhkin, Calcium Orthophosphate Coatings, Films and Layers, *J. Funct. Biomater.*, 2012, 1, p 22-107
8. M. Roy, B.V. Krishna, A. Bandyopadhyay, and S. Bose, Laser Processing of Bioactive Tricalcium Phosphate Coating on Titanium for Load-Bearing Implants, *Acta Biomater.*, 2008, 4, p 324-333
9. S.J. Ding, C.P. Ju, and J.H. Lin, Characterization of Hydroxyapatite and Titanium Coatings Sputtered on Ti-6Al-4V Substrate, *J. Biomed. Mater. Res.*, 1999, 44(3), p 266-279
10. S.V. Dorozhkin, Calcium Orthophosphate Coatings, Films and Layers, *J. Funct. Biomater.*, 2012, 1, p 1-40
11. S. Nag, S.R. Paital, P. Nandawana, K. Mahdak, Y.H. Ho, H.D. Vora, R. Banerjee, and N.B. Dahotre, Laser Deposited Biocompatible Ca-P Coatings on Ti-6Al-4V: Microstructural Evolution and Thermal Modelling, *Mater. Sci. Eng. C.*, 2013, 33, p 165-173
12. I-S. Lee, C-N. Chang, H-E. Kim, J-C. Park, J.H. Song, and S-R. Kim, Various Ca/P Ratios of Thin Calcium Phosphate Films, *Mater. Sci. Eng. C.*, 2002, 22, p 15-20



13. M. Tlotleng, E. Akinlabi, M. Shukla, and S. Pityana, Microstructures, Hardness and Bioactivity of Hydroxyapatite Coatings Deposited by Direct Laser Melting Process, *J. Mater. Sci. Eng. C*, 2014, **43**, p 189-198
14. D. Liu, K. Savino, and M.Z. Yates, Coating of Hydroxyapatite Films on Metal Substrates by Seeded Hydrothermal Deposition, *Surf. Coat. Technol.*, 2011, **205**, p 3975-3986
15. R. Sultana, J. Yang, and X. Hu, Deposition of Micro-Porous Hydroxyapatite/Tri-Calcium Phosphate Coating on Zirconia-Based Substrate, *J. Am. Ceram. Soc.*, 2012, **95**(4), p 1212-1215
16. G.J. Cheng, D. Pirzada, M. Cai, P. Mohanty, and A. Bandyopadhyay, Bioceramic Coating of Hydroxyapatite on Titanium Substrate with Nd:YAG Laser, *Mater. Sci. Eng. C*, 2005, **25**, p 541-547
17. D.G. Wang, C.Z. Chen, J. Ma, and G. Zhang, In Situ Synthesis of Hydroxyapatite Coating by Laser Cladding, *Colloids Surf., B*, 2008, **66**, p 155-162
18. S.V. Dorozhkin, Calcium Orthophosphate Coatings, Films and Layers, *Prog. Biomater.*, 2010, **1**(1), p 1-40
19. M. Roy, A. Bandyopadhyay, and S. Bose, Induction Plasma Sprayed Nano Hydroxyapatite Coatings on Titanium for Orthopaedic and Dental Implants, *Surf. Coat. Technol.*, 2008, **205**(8-9), p 2785-2792
20. D.J. Blackwood and K.H.W. Seah, Electrochemical Cathodic Deposition of Hydroxyapatite: Improvements in Adhesion and Crystallinity, *Mater. Sci. Eng. C*, 2009, **29**, p 1233-1238
21. D.-M. Liu, Q. Yang, and T. Troczynski, Sol-Gel Hydroxyapatite Coatings on Stainless Steel Substrates, *Biomaterials*, 2002, **23**, p 691-698
22. V. Kokenyesi, I. Popovich, M. Kikineshi, L. Daroczi, D. Beke, Y. Sharkany, and C.S. Hegedus, Preparation of Calcium Phosphate Coatings on Titanium by Pulse Nd:YAG Laser Processing, *Opto-Electro. Adv. Mater. Rapid. Commun.*, 2007, **1**(4), p 171-175
23. R.A. Ismail, E.T. Salim, and W.K. Hamoudi, Characterization of Nanostructured Hydroxyapatite Prepared by Nd:YAG Laser Deposition, *Mater. Sci. Eng. C*, 2013, **33**, p 47-52
24. D. Wang, C. Chen, J. Ma, and T. Lei, Microstructure of Yttrium Calcium Phosphate Bioceramic Coatings Synthesized by Laser Cladding, *Appl. Surf. Sci.*, 2007, **253**, p 4016-4020
25. C.S. Chien, T.J. Han, T.F. Hong, T.Y. Kuo, and T.Y. Liao, Effects of Different Binders on Microstructure and Phase Composition of Hydroxyapatite Nd-YAG Laser Clad Coatings, *Mater. Trans.*, 2009, **50**(12), p 2852-2857
26. K.A. Gross and C.C. Berndt, Thermal Processing of Hydroxyapatite for Coating Production, *J. Biomed. Mater. Res.*, 1998, **39**(4), p 580-587
27. A. Choudhuri, P.S. Mohaunty, and J. Karthikeyan, Bio-ceramic Composite Coatings by Cold Spray Technology, Thermal Spraying, 2009, p 391-396
28. X. Zhou and P. Mohanty, Electrochemical Behaviour of Cold Sprayed Hydroxyapatite/Titanium Composite in Hanks' Solution, *Electrochim. Acta*, 2012, **65**, p 134-140
29. M.R. Mansur, J. Wang, and C.C. Berndt, Microstructure, Composition and Hardness of Laser-Assisted Hydroxyapatite and Ti-6Al-4V Composite Coatings, *Surf. Coat. Technol.*, 2013, **232**, p 482-488
30. C.S. Chien, T.F. Hong, T.J. Han, T.Y. Kuo, and T.Y. Liao, Effects of Different Binders on Microstructure and Phase Composition of Hydroxyapatite Nd-YAG Laser Clad Coatings, *Appl. Surf. Sci.*, 2011, **257**(6), p 2387-2393
31. M. Bray, A. Cockburn, and W. O'Neill, The Laser-Assisted Cold Sprayed Process and Deposition Characterisation, *Surf. Coat. Technol.*, 2009, **203**, p 2851-2857
32. E.O. Olakanmi, M. Tlotleng, C. Meacock, S. Pityana, and M. Doyoyo, Deposition Mechanism and Microstructure of Laser-Assisted-Cold-Sprayed (LACS) Al-12 wt.%Si Coatings: Effects of Laser Power, *JOM*, 2013, **65**(6), p 776-783
33. R. Lupoi, M. Sparkes, A. Cockburn, and W. O'Neill, High Speed Titanium Coatings by Supersonic Laser Deposition, *Mater. Lett.*, 2011, **65**, p 3205-3207
34. F.J. Brodmann, Cold Spray Process Parameters: Powders, *The Cold Spray Materials Deposition Process*, V.K. Champagne, Ed., Woodhead Publishing, 2007, p 105-116
35. E.O. Olakanmi and M. Doyoyo, Laser-Assisted Cold-Sprayed Corrosion and Wear-Resistant Coatings: A Review, *J. Therm. Spray Technol.*, 2014, **23**(5), p 765-785
36. K.A. Khor, H. Li, and P. Cheang, Significance of Melt-Fraction in HVOF Sprayed Hydroxyapatite Particles, Splats and Coatings, *Biomaterials*, 2004, **25**(7-8), p 1177-1186
37. W.E. Brown and E.F. Epstein, Crystallography of Tetracalcium Phosphate, *J. Res. Nat. Bureau Std. A. Phys. Chem.*, 1965, **69**(6), p 547-551
38. H. Li, K.A. Khor, and P. Cheang, Thermal Sprayed Hydroxyapatite Splats: Nanostructures Pore Formation Mechanisms and TEM Characterisation, *Biomaterials*, 2004, **25**, p 3463-3471